Evaluating Hardening Laws at Large Tensile Strains in Sheet Specimens

R. A. AYRES

In the finite element modeling of sheet metal formability, the strains in the sheet are calculated from a hardening law which is normally derived from a tensile test. These laws are known to be accurate only up to the maximum uniform strain in tension. However, they are extrapolated during modeling to strains three to five times greater than the uniform strain. In assessing the applicability of these hardening laws at large strains, tensile specimens of 1008 AK steel and commercial purity titanium and zinc were gridded with a fine mesh and slowly pulled to failure. During the test, photographs were taken of the deforming grid in order to develop a complete strain and strain-rate history for each element across the minimum cross section. These data were combined with a hardening law for each material to calculate the total axial load on the specimen. Good agreement between the calculated and measured loads suggests that hardening laws for these materials can be extrapolated to large strains.

I. INTRODUCTION

IN the modeling of sheet metal deformation, it is necessary to have an accurate description of a material's hardening law for several reasons. The first consideration is to predict accurate loads in the press and strains in the part. The other reasons are concerned with assessing the effect of other variables, which are more difficult to measure, on the deformation process. Examples of these other variables may include friction, temperature gradients, and a changing shape of the yield surface with strain.[1]

An accurate, useful hardening law must relate the material's flow stress over a wide range of strains up to localized necking strains. For rate sensitive metals (*e.g.*, steel, titanium, and zinc) the limit strains are generally well beyond the maximum uniform strain found in a tensile test. To measure flow stress at these post-uniform strains requires that the effect of necking be included. For cylindrically shaped tensile samples, Bridgman[2] has derived an expression, based on the neck contour, to correct the average true stress measured at the neck to an effective value of stress where plastic flow actually takes place.

A simple analysis does not exist for flat sheet samples since the geometry of the neck is much more complex. An early stress analysis of necking in a flat specimen by Aronofsky[3] uses a hybrid approach where a hardening law from a cylindrical specimen is combined with a strain distribution in the sheet specimen. The strain distribution was measured from an initially square mesh scribed in the specimen. Although this analysis was performed on a steel sample, the hardening law did not include a rate dependent term.

A more recent attempt to evaluate strain hardening at large strains in sheet specimens was presented by Saka, Painter, and Pearce.[4] In this work the authors photo-printed a 1 mm square grid on steel and titanium specimens and pulled them to failure. During the test the tensile load was recorded and the grid was periodically photographed to provide a complete description of the strain distribution up to failure. From this data the authors provided an analysis based on plasticity, assuming proportional loading, to isolate the tensile load acting only on the central element in the necked region of the specimen. From these data a log-log plot was made of the true stress and strain to obtain the strain hardening exponent, n, (from $\sigma = K\varepsilon^n$) at strains well into the diffuse neck. This plot was corrected for an increase in strain rate of the central element during necking by assuming $\sigma = K\dot{\varepsilon}^m$ where $\dot{\varepsilon}$ is the strain rate and m is the strain-rate sensitivity. From this work the authors found n to increase from the maximum uniform strain to diffuse necking by ~14 pct for steel and ~100 pct for titanium.

The current study is similar to that of Saka, Painter, and Pearce[4] but with some important differences. This study evaluates a proposed hardening law at large strains over the entire cross section of the sample. This approach eliminates the inherently inaccurate procedure of isolating the part of the total load operating only on the central element of the sample. The proposed hardening laws evaluated here are derived by a best fit to the tensile data during uniform strain, and no restriction is placed on the form of the law (*e.g.*, $\sigma = K\varepsilon^n\dot{\varepsilon}^m$ used by Saka *et al.*). The plasticity analysis for the stress calculation does not assume proportional loading of the elements in the necked region and, instead, uses the incremental theory of plasticity. Three different sheet materials with varying amounts of post-uniform strain are evaluated: 1008/1010 AK steel, commercially pure titanium, and a zinc alloy.

II. ANALYSIS

The calculation scheme is to compare the measured load imposed on the specimen to the calculated load based on a plasticity theory and a hardening law for that specimen. The independent variable in this study is time, since the test is carried out at a constant cross head rate. Therefore, both the measured and calculated loads can be compared at the same increments of time throughout the test.

A schematic of the gridded tensile sample is shown in Figure 1, where the grids reflect the necked region. It is assumed that the grid mesh is sufficiently fine that the strains ε_1 and ε_2 are constant through a given element i. Furthermore, only the loads in the elements located at the

R. A. AYRES is Senior Staff Research Scientist with General Motors Research Laboratories, Warren, MI 48090-9055.

Manuscript submitted December 8, 1981.

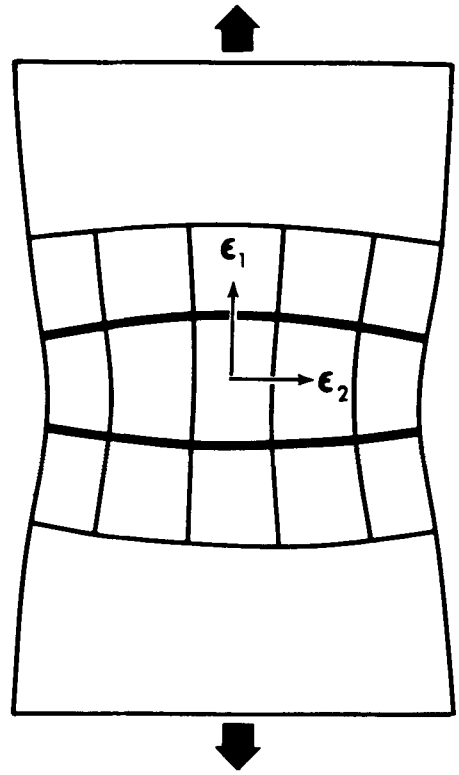

Fig. 1 — Schematic of gridded tensile sample showing a deformed grid pattern at the minimum cross section of the neck.

minimum cross section will be calculated. Therefore, it is assumed that the principal strains ε_1 and ε_2 remain parallel and transverse to the tensile axis, respectively, up to the onset of the through-thickness neck.

The plasticity analysis described below assumes planar isotropy, plane stress, rigid-plastic behavior, and isotropic hardening of the yield surface. The more general elastic-plastic treatment of plasticity is described by Wang and Wenner.[5] The shape of the yield surface is modified according to Hill[6] to include the effect of normal anisotropy. The basic equations of deformation, from the incremental theory of plasticity, are defined in terms of strain rate as shown below.

$$\dot{\varepsilon}_1 = \frac{\dot{\bar{\varepsilon}}}{\bar{\sigma}}(\sigma_1 - c\sigma_2) \qquad [1]$$

$$\dot{\varepsilon}_2 = \frac{\dot{\bar{\varepsilon}}}{\bar{\sigma}}(\sigma_2 - c\sigma_1)$$

In these equations $\dot{\varepsilon}_1$ and $\dot{\varepsilon}_2$ are the true strain rates of the principal strains in a given element shown in Figure 1. Similarly, σ_1 and σ_2 are the true stresses acting in the same directions as $\dot{\varepsilon}_1$ and $\dot{\varepsilon}_2$. The c term includes the normal anisotropy parameter, r, as shown in Eq. [2].

$$c = \frac{r}{1 + r} \qquad [2]$$

The terms $\dot{\bar{\varepsilon}}$ and $\bar{\sigma}$ are the effective strain rate and effective stress as defined in Eqs. [3] and [4].

$$\dot{\bar{\varepsilon}} = \frac{1 + r}{\sqrt{1 + 2r}}(\dot{\varepsilon}_1^2 + \dot{\varepsilon}_2^2 + 2c\dot{\varepsilon}_1\dot{\varepsilon}_2)^{1/2} \qquad [3]$$

$$\bar{\sigma} = (\sigma_1^2 + \sigma_2^2 - 2c\sigma_1\sigma_2)^{1/2} \qquad [4]$$

To calculate the effective strain, Eq. [3] must be integrated over time, t.

$$\bar{\varepsilon} = \int_0^t \dot{\bar{\varepsilon}}dt \qquad [5]$$

The relationship between $\bar{\sigma}$, $\bar{\varepsilon}$, and $\dot{\bar{\varepsilon}}$ is the hardening law determined from a tensile test.

$$\bar{\sigma} = F(\bar{\varepsilon},\dot{\bar{\varepsilon}}) \qquad [6]$$

By combining Eqs. [1] and [5] the true axial stress in each element can be calculated from Eq. [7].

$$\sigma_{1(i)} = \frac{F(\bar{\varepsilon},\dot{\bar{\varepsilon}})}{(1 - c^2)\dot{\bar{\varepsilon}}_{(i)}}(\dot{\varepsilon}_{1(i)} + c\varepsilon_{2(i)}) \qquad [7]$$

The only data required are the strain and strain rate history of the ith element. The total load carried in each element, P_i, is calculated from $\sigma_{1(i)}$ and the original cross sectional area of the ith element as shown in Eq. [8].

$$P_i = A_{0(i)}\sigma_{1(i)} \exp(-\varepsilon_{1(i)}) \qquad [8]$$

The total load imposed on the specimen is the summation of $P_{(i)}$ for each element at the same instant of time.

$$P_{\text{total}} = \sum_{i=1}^{i=n} P_{(i)} \qquad [9]$$

Implicit in this analysis is the assumption that the deformation in each element is independent of its neighbor. Therefore, the sample deforms as a flat bundle of fibers. The overall geometry of the neck is not accounted for, since the loads in the sample are calculated only at the minimum cross section. The effect of the neck on the load required for deformation is accounted for because the ratio of $\varepsilon_2/\varepsilon_1$ changes in each element from the edge to the center of the specimen. Therefore, the elements near the center require a higher load for deformation to continue since they are nearer plane strain.

III. EXPERIMENTAL PROCEDURE

The three sheet materials investigated in this study included 1008/1010 AK steel, commercial purity titanium, and a zinc alloy designated #101 by the Ball Corporation. The nominal composition of the alloy elements in zinc in weight percent are Cd (0.04 to 0.06), Pb (0.06 to 0.08), Fe (≤0.008), Cu (≤0.002). The thickness of these materials is 1.0 mm for steel and titanium and 0.88 mm for zinc. These sheet materials were selected because they presented a range of behavior of strain and strain-rate hardening, normal anisotropy, and post-uniform strain.

The hardening laws of the sheet metals were obtained from standard ASTM, E-8, tensile samples with a gage length of 50.8 mm and a tensile axis parallel to the rolling direction of the sheet. To determine the hardening laws from measurements of stress *vs* strain, samples were pulled at initial strain rates of 2.1×10^{-5} s^{-1}, 2.1×10^{-4} s^{-1}, and 2.1×10^{-3} s^{-1}, except for steel which was also pulled at 2.1×10^{-6} s^{-1}. These strain rates were selected to insure that the specimens remained at ambient temperatures of 22 to 24 °C throughout the test.

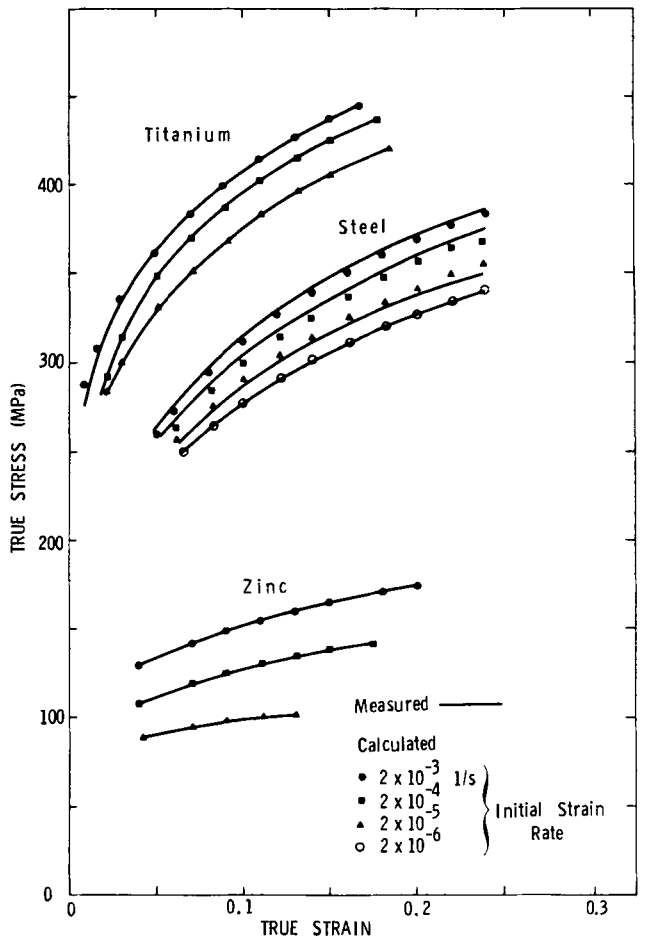

Fig. 2—Plot of true stress *vs* true strain for the materials evaluated. The solid lines are the measured data up to the maximum load, whereas the dots are calculated from the respective hardening laws of the materials.

The complete strain and strain rate history of each element of the tensile sample was accomplished by first photoprinting a 0.51 mm square grid on the gage section. Since the specimens were ~12.7 mm wide, the grid divided the gage section into 25 elements or fibers. Then the specimens were pulled to failure, except for zinc, at an initial crosshead rate of 2.9×10^{-5} s^{-1} while simultaneously recording load and taking pictures of the grid at various increments of time. The zinc test was stopped due to the presence of an edge crack.

Analytical expressions for the strain history were obtained by a least-squares, cubic spline fit to strains beyond maximum load from plots of ε_1 and ε_2 *vs* time. For strains up to the maximum load, ε_1 and ε_2 were expressed as a linear function of time. This procedure was performed on an interactive computer terminal. These expressions were then differentiated with respect to time, at selected values of time, and fit to another least-squares cubic spline to obtain $\dot{\varepsilon}_{1(i)}$ and $\dot{\varepsilon}_{2(i)}$ *vs* time. This calculational procedure was performed for only half of the elements, from the center to the specimen edge, because of symmetry. Additional calculations of the edge element were made to measure r [from $r = -\varepsilon_2/(\varepsilon_1 + \varepsilon_2)$] to large strains, since the edge element is in uniaxial tension beyond maximum load.

IV. RESULTS

The hardening laws for all three materials were calculated from the tensile data shown in Figure 2. Each solid curve was approximated initially by a least squares fit to $\sigma = k\varepsilon^n$ by assuming that the strain rate change within the test was negligible. Figure 2 shows that there is no systematic deviation between the calculated and measured values of stress as a function of strain within the uniform strain region at strains $\gtrsim$2 pct. If a deviation is measured, then another form of $\sigma = f(\varepsilon)$ must be derived. The strain rate dependency of the hardening laws was determined by evaluating the K and n terms for each material as indicated below. In all cases the units of σ and K are MPa.

1008/1010 AK Steel: For steel, n increased only 4.3 pct as the strain rate decreased from $\sim 10^{-3}$ to 10^{-6} s^{-1}. Since this change in n with strain rate is small, n was assumed constant at an average value of 0.239. The K term was a stronger function of strain rate and was determined from semi-log plots of K *vs* log $\dot{\varepsilon}$ for several levels of strain. A linear fit of K from this semi-log plot gave a relationship of $K = 586.6 + 8.08 \ln \dot{\varepsilon}$. Therefore, the final hardening law for steel is shown in Eq. [10].

$$\textit{steel}\ \sigma = 586.6\varepsilon^{0.239}(1 + 0.014 \ln \dot{\varepsilon}) \qquad [10]$$

A comparison of this law to the actual data is shown in Figure 2 with the dots representing Eq. [10]. It is clear that the calculated results closely parallel the actual data at strains $\gtrsim$0.07. However, the gap in the flow curves between the strain rates of 2.9×10^{-5} and 2.9×10^{-4} s^{-1} has been eliminated by Eq. [10] due to the averaging procedure of the K and n terms.

Titanium and Zinc: Both of these materials exhibited a significant dependence of K and n on strain rate. From semi-log plots of K and n *vs* log $\dot{\varepsilon}$, the best fit through the data was a quadratic equation of the form K, $n = A(\ln \dot{\varepsilon})^2 + B \ln \dot{\varepsilon} + C$. Therefore, the hardening laws for both of these materials were of the form $\sigma = K\varepsilon^n$, where K and n are functions of strain rate as shown in Eqs. [11] and [12].

$$\sigma = K(\dot{\varepsilon})\varepsilon^{n(\dot{\varepsilon})}$$

where

titanium

$$K = -2.12(\ln \dot{\varepsilon})^2 - 27.99 \ln \dot{\varepsilon} + 505.22$$
$$n = -8.49 \times 10^{-4}(\ln \dot{\varepsilon})^2 - 0.0175 \ln \dot{\varepsilon} + 0.0906 \qquad [11]$$

zinc

$$K = -3.1367(\ln \dot{\varepsilon})^2 - 25.06 \ln \dot{\varepsilon} + 205.14$$
$$n = -6.49 \times 10^{-3}(\ln \dot{\varepsilon})^2 - 83.47 \times 10^{-3} \ln \dot{\varepsilon} - 0.0604 \qquad [12]$$

A comparison of the calculated flow stress to measured values in Figure 2 shows excellent agreement with the measured flow stress overall rates. These hardening laws from Eqs. [10], [11], and [12] represent the expressions which will be used in the analysis as Eq. [6].

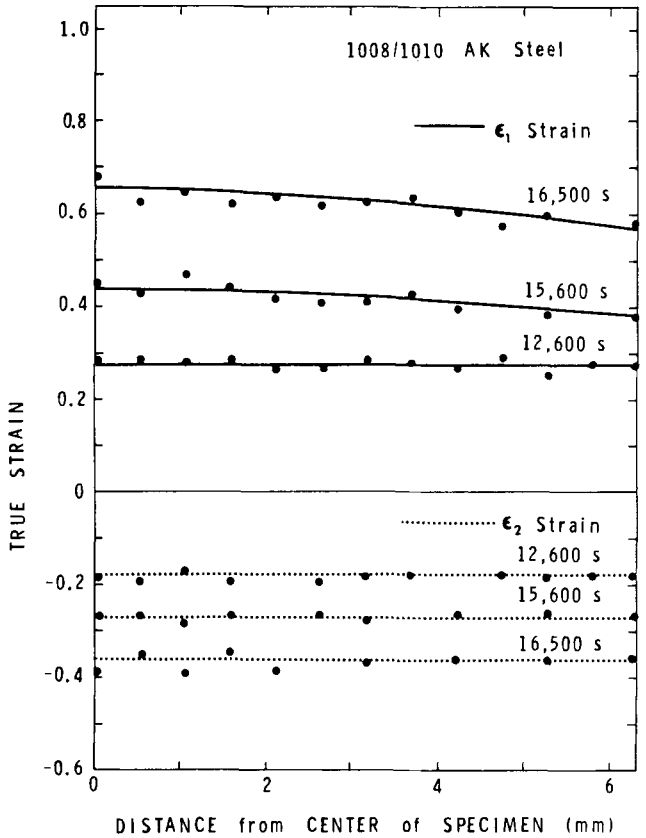

Fig. 3—Plot of the ε_1 and ε_2 strains across the specimen width at various increments of time for 1008/1010 AK steel.

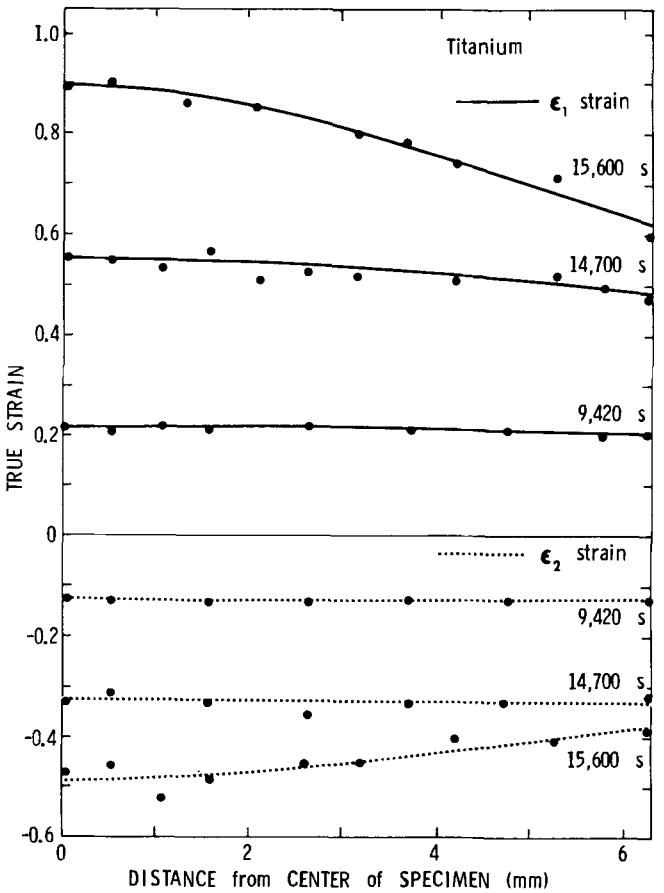

Fig. 5—Plot of the ε_1 and ε_2 strains across the specimen width at various increments of time for titanium.

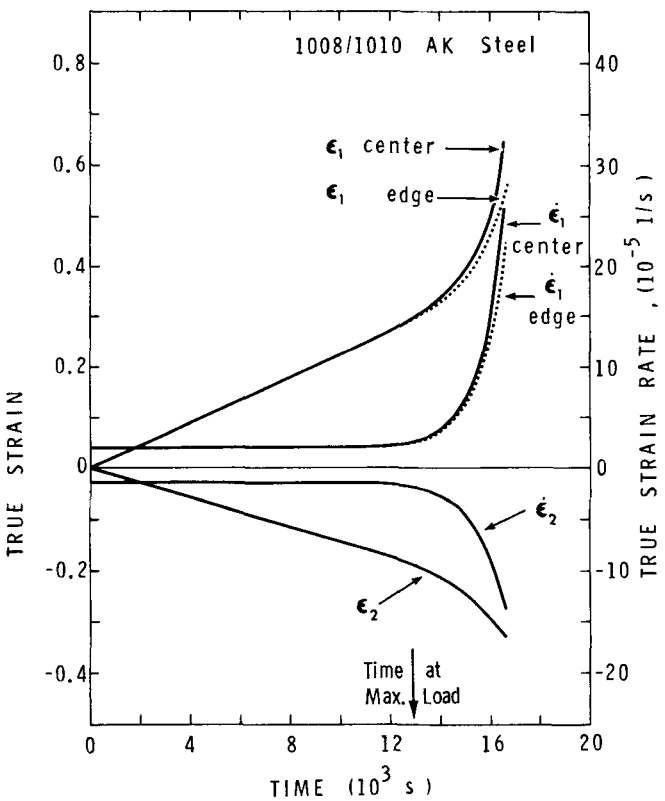

Fig. 4—Plot of the ε_1 and $\dot{\varepsilon}_1$ values *vs* time for elements at the center and at the edge of the tensile specimen for 1008/1010 AK steel. There was no gradient from center to edge for ε_2 and $\dot{\varepsilon}_2$.

The second phase of the results were measurements of r to large strains, as well as the strain and strain-rate history of a tensile specimen. These data were obtained from the measurements of strain at the minimum cross section of the sample as discussed below for each material.

1008/1010 AK Steel

A plot of the ε_1 and ε_2 strains across the minimum cross section of the specimen is shown in Figure 3. Both strains remain uniform across the cross section up to the maximum load at 12,600 seconds. Beyond 12,600 seconds the ε_1 strain slowly develops a gradient from center to edge, while the ε_2 strain remains essentially constant across the width. From the ε_1 and ε_2 at the edge element, the r value can be determined up to large strains from $r = -\varepsilon_2/(\varepsilon_1 + \varepsilon_2)$, because the edge remains in uniaxial tension. For steel, r remained virtually constant at ~1.8 up to strains of $\varepsilon_1 = 0.6$.

The strain and strain-rate history of all the elements was determined from the data in Figure 3 as indicated for the center and edge elements in Figure 4. All of the elements are assumed to deform at the same strain rate up to the maximum load. Beyond maximum load, the data are fit initially to a least squares cubic curve to describe analytically $\varepsilon_{1(i)}$ and $\varepsilon_{2(i)}$ *vs* time. Differentiating the curve at several points and again fitting to a least squares cubic curve gives $\dot{\varepsilon}_{1(i)}$ and $\dot{\varepsilon}_{2(i)}$ *vs* time. Figure 4 shows that the central element increases its strain rate by a factor of ~17 from the initial strain rate to just prior to through thickness necking.

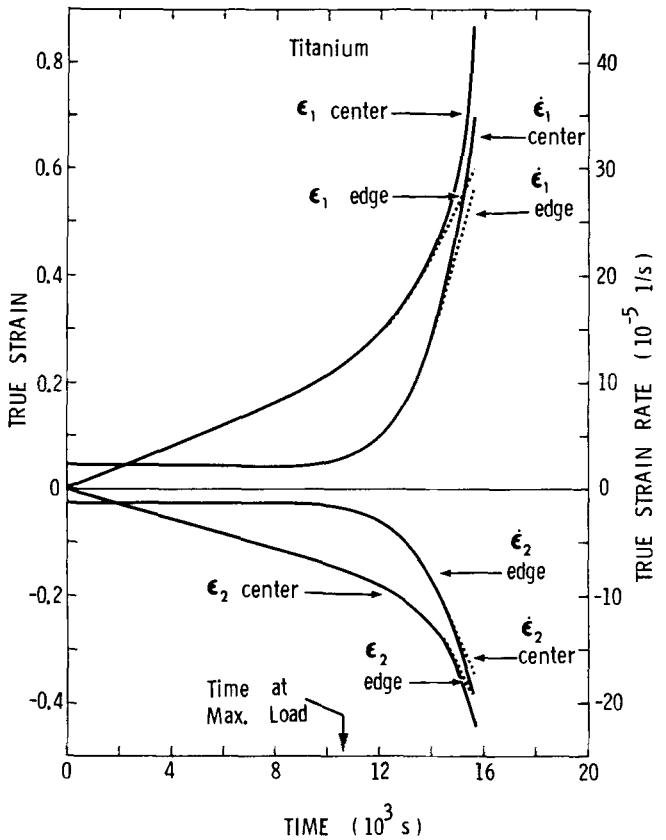

Fig. 6—Plot of the ε_1, $\dot{\varepsilon}_1$ and ε_2, $\dot{\varepsilon}_2$ values *vs* time for elements at the center and edge of the tensile specimen for titanium.

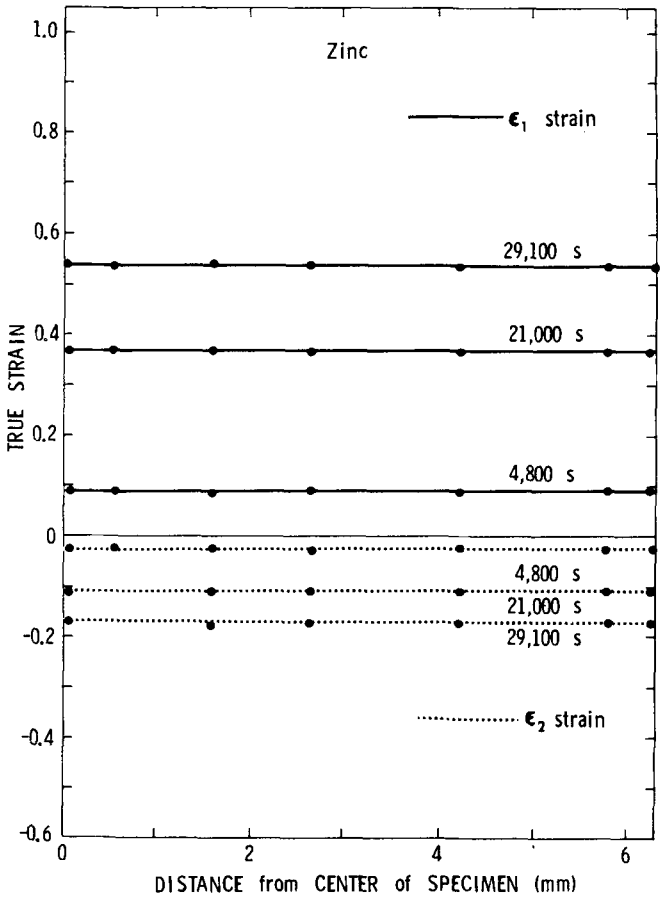

Fig. 7—Plot of the ε_1 and ε_2 strains across the specimen width at various increments of time for zinc.

Titanium

Plots of ε_1 and ε_2, across the specimen width, are shown in Figure 5 at various increments of time. These strains are similar to those of steel, except at larger strains where both ε_1 and ε_2 develop significant gradients from center to edge. The r value in the rolling direction, again, remains relatively constant through the test at a value of 1.86. The strain and strain-rate behavior of the center and edge elements are fitted to a least square cubic curve in similar manner to steel. These data are shown in Figure 6.

Zinc

The zinc material displayed the most unusual behavior of the three materials evaluated, since no gradient developed across the width in either the ε_1 or ε_2 strains (Figure 7). The high strain rate sensitivity of this material kept the gage section quite uniform well past the maximum load,[7] even though the sample was pulled for the longest time. The test was terminated for this material because of an edge crack and not because of a through thickness neck. Measurements of r showed it to remain constant at ~0.44 at strains $>\varepsilon_1 = 0.14$. The plots of strain and strain-rate history are shown in Figure 8 for only one element, which represents all 25 elements. Since the increase in strain and strain-rate with time is very gradual beyond maximum load, in contrast to steel and titanium, a single cubic equation satisfactorily fit all the data.

Computations

A computer program was written that consisted of two nested DO loops. The inner loop calculated $P_{(i)}$ from Eq. [8]

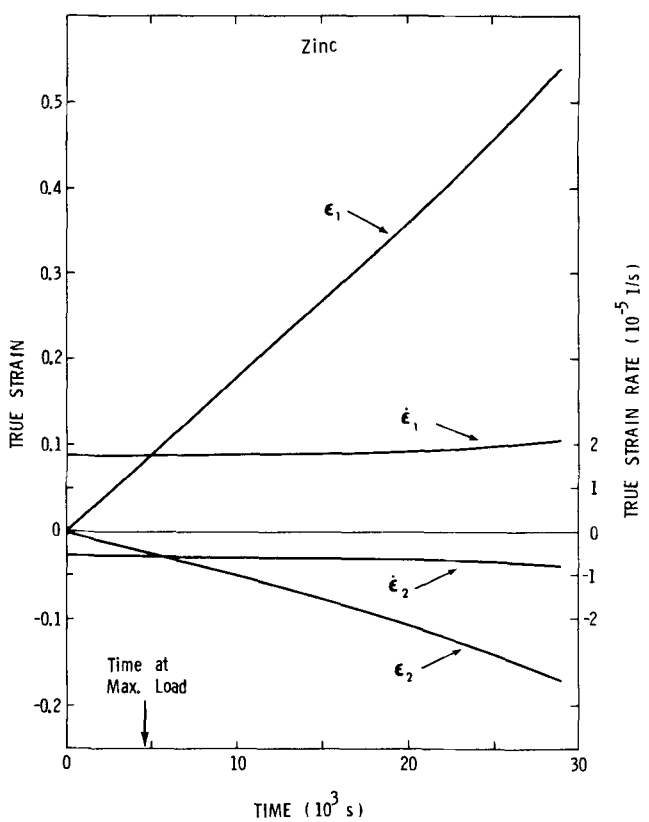

Fig. 8—Plot of the ε_1 and $\dot{\varepsilon}_1$ and ε_2, $\dot{\varepsilon}_2$ values *vs* time for all the elements in the zinc specimen. No gradients in strain were measured from the center in the edge of the tensile specimen.

for given intervals of time, and the outer loop calculated the total load on the specimen from Eq. [9]. The interval of time was always kept at 1/100 of the total time of the test. This interval was sufficiently small for the numerical integration of $\bar{\varepsilon}$ from Eq. [5] so that a smaller interval would not be expected to affect the results.

It is important to note that while the computations included the analytical expressions for $\varepsilon_{1(i)}$ and $\dot{\varepsilon}_{1(i)}$ in a straightforward manner, such a procedure was not possible for $\varepsilon_{2(i)}$ and $\dot{\varepsilon}_{2(i)}$. The ratio of $\dot{\varepsilon}_2/\dot{\varepsilon}_1$ is very sensitive to the approximation procedure and will cause oscillations in the load *vs* time curve beyond maximum load. To eliminate this computational difficulty, an expression was found in an iterative procedure that allowed $\dot{\varepsilon}_2/\dot{\varepsilon}_1$ to vary smoothly during diffuse necking and reproduce the original $\dot{\varepsilon}_{2(i)}$ within 5 pct when multiplied by $\dot{\varepsilon}_{1(i)}$.

The final plots of load *vs* time comparing the calculated load to the measured load are shown in Figures 9 through 11. The post-uniform strain region has been magnified for the steel and titanium for closer comparison. It is important to note that strain is not constant across the width of the sample in these materials for a given value of time. Therefore, the range of strain can be determined by referring to Figures 3, 4, 5, and 6, which plot ε_1 *vs* time from center to edge. For the steel the ε_1 range at the last increment of time (16,500 seconds) is from 0.57 at the edge to 0.65 at the center. The strain range is even greater for titanium at 15,600 seconds with ε_1 varying from 0.63 to 0.92. The zinc alloy has no strain gradient, and its maximum value of ε_1 is 0.54 at 29,100 seconds. The sensitivity of the load *vs* time calculations to changes in n and K is shown by the error bars in Figures 9 through 11. For all three materials the range of the error bar corresponds to changing both n and K by ±10 pct.

V. DISCUSSION

The close agreement between the calculated and measured tensile loads in Figures 9 through 11 suggests that hardening laws can be extrapolated to strains four to five times larger than uniform strain. It is important, however, not to extrapolate these laws to testing regimes beyond those from which the laws are derived. As an example, Wagoner has shown[8] that the strain-rate sensitivity for 1008/1010 AK steel becomes a strong function of strain rate at rates $>10^{-3}$ s^{-1}. Therefore, a different form of a hardening law must be derived for these higher strain rates. In addition, the effect of thermal gradients on deformation may need to be included at higher rates.

At strains beyond maximum load, strain gradients across the specimen width change the strain state from pure tension at the edges, where $\dot{\varepsilon}_2/\dot{\varepsilon} = -r/(1+r)$, to a state approaching but never reaching plane strain at the center, where $\dot{\varepsilon}_2/\dot{\varepsilon}_1 = 0$. To calculate the stress in each element, except at the edges, requires an assumption about the shape of the yield surface. If the actual shape differs from the assumed elliptical shape, from Eqs. [3] and [4], then an error could be introduced in the stress that is independent of the hardening law. While this change of strain state is greatest in the center element, true plane strain is never reached prior to the formation of a thickness neck. The plots of $\dot{\varepsilon}_1$ and $\dot{\varepsilon}_2$ for the center elements in Figures 4, 6, and 8 shows

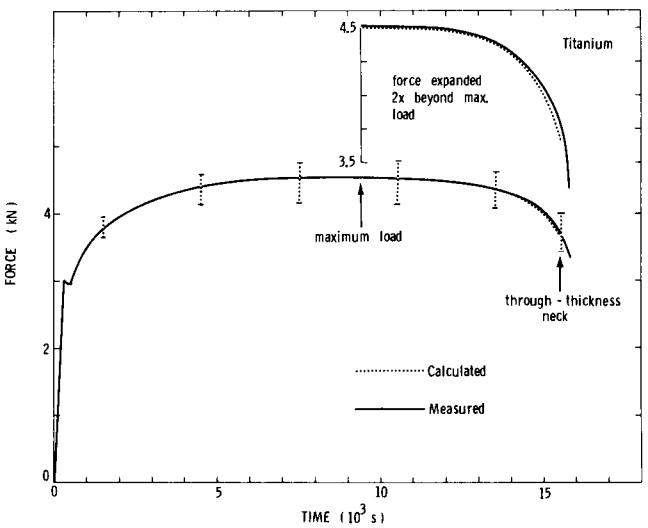

Fig. 10—Comparison of measured load to the calculated load *vs* time in the titanium specimen. The error bars show the sensitivity of the calculated load to changes of ±10 pct in the n and K values from Eq. [11].

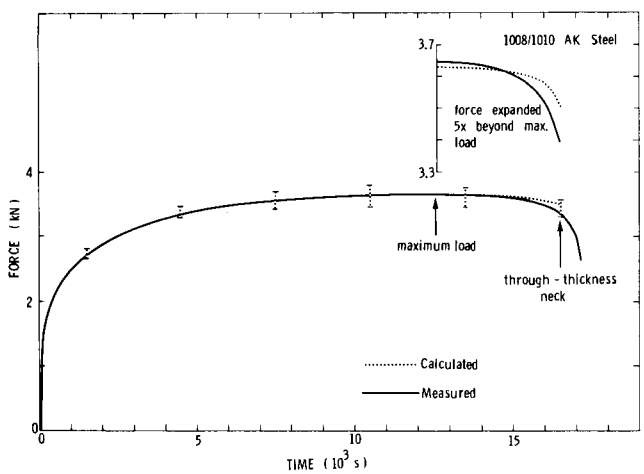

Fig. 9—Comparison of the measured load to the calculated load *vs* time in the 1008/1010 steel specimen. The error bars show the sensitivity of the calculated load to changes of ±10 pct in the n and K values from Eq. [10].

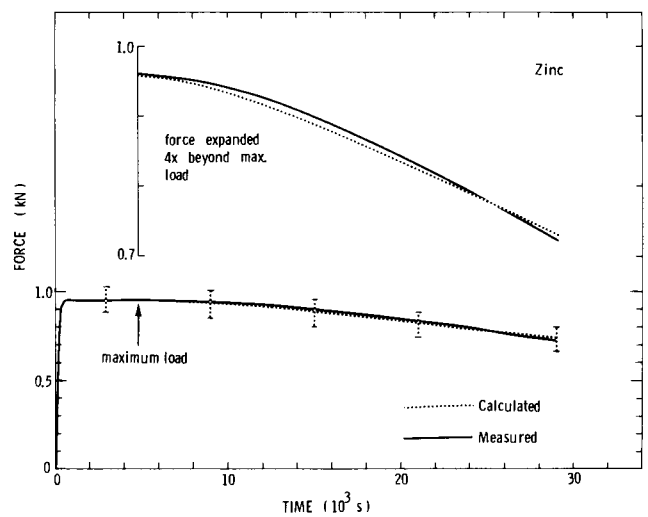

Fig. 11—Comparison of measured load to the calculated load *vs* time in zinc specimen. The error bars show the sensitivity of the calculated load to changes of ±10 pct in the n and K values from Eq. [12].

that $\dot{\varepsilon}_2$ is increasingly more negative for larger values of $\dot{\varepsilon}_1$. Therefore, any error in the calculated load due to the shape of the yield surface, used in the analysis, should be small since the range of strain states is small. The strain remains tensile at the specimen edge and is intermediate between plane strain and tensile for the center element at the highest strains. This observation was reported in the earlier work of Saka, Painter, and Pearce.[4]

As stated earlier, this study is similar to the earlier study by Saka, Painter, and Pearce[4] in the experimental procedure, but differs in the details of the analysis. In this study n is assumed to be constant with strain, whereas Saka *et al.* measure n as a function of strain. For steel, either investigation shows that n is at best a small function of strain. This is true despite slight differences in the form of the hardening law and differences in the initial strain rate ($\sim 10^{-2}$ s^{-1} for Saka and $\sim 10^{-5}$ s^{-1} for this study). However, this investigation disagrees with the earlier results for titanium where n is reported to increase ~100 pct in diffuse necking as a function of strain. In contrast, this study shows excellent agreement between the calculated and measured loads from Eq. [11] by allowing $n_{(\dot{\varepsilon})}$ to decrease and $K_{(\dot{\varepsilon})}$ to increase with strain rate. While the $n_{(\dot{\varepsilon})}$ is not the same as the rate independent n from Saka *et al.*, Eq. [11] does show that it is not necessary for n to be a function of strain if the strain rate dependency is properly accounted for. A direct observation of a similar increase with strain in the apparent n during diffuse necking that is actually a strain rate effect has been reported by Wagoner[9] for a Zn alloy.

VI. CONCLUSIONS

1. Tensile hardening laws, derived from the uniform strain region for sheet 1008/1010 AK steel, titanium, and zinc, can be extrapolated to tensile strains four to five times greater than the maximum uniform strain.
2. The accuracy of these extrapolations would be expected to decrease if a hardening law is applied to a testing regime (strain rate, temperature) other than the regime from which the law was derived.
3. The application of the r-value corrected, isotropically hardening yield surface with the incremental theory of plasticity successfully calculated stress over large values of tensile strain for materials with widely varying flow behavior.

ACKNOWLEDGMENTS

The author appreciates the numerous, stimulating conversations with Dr. M. L. Wenner throughout this investigation. The assistance of Mr. J. C. Price in the computer programming and Mr. P. L. Frechette in the tensile testing is gratefully acknowledged.

REFERENCES

1. R. H. Wagoner: *Metall. Trans. A*, 1980, vol. 11A, p. 165.
2. P. W. Bridgman: *Trans. ASM*, 1944, vol. 32, p. 553.
3. J. Aronofsky: *J. Appl. Mech.*, 1951, vol. 18, p. 75.
4. K. Saka, M. J. Painter, and R. Pearce: *J. Mechanical Working Technology*, 1979, vol. 3, p. 17.
5. N. -M. Wang and M. L. Wenner: Symposium on the *Mechanics of Sheet Metal Forming*, D. P. Koistinen and N. -M. Wang, eds., Plenum Press, New York, NY, 1978, p. 367.
6. R. Hill: *Mat. Proc. Camb. Phil. Soc.*, 1979, vol. 85, p. 179.
7. A. K. Ghosh: *Metall. Trans. A*, 1977, vol. 8A, p. 1221.
8. R. H. Wagoner: *Scripta Met.*, 1981, vol. 15, p. 1135.
9. R. H. Wagoner: *Metall. Trans. A*, 1981, vol. 12A, p. 71.